Wetting transition from hydrophilic to superhydrophobic over dendrite copper leaves grown on steel meshes

Raziyeh Akbari, Guilhem Godeau, Mohammadreza Mohammadizadeh, Frédéric Guittard, Thierry Darmanin

Wetting transition from hydrophilic to superhydrophobic over dendrite copper leaves grown on steel meshes

Raziyeh Akbari[1,2], Guilhem Godeau[2], Mohammadreza Mohammadizadeh[1], Frédéric Guittard[2], and Thierry Darmanin[*,2]

1. Supermaterial Research Lab (SRL), Department of Physics, University of Tehran, North Kargar Av., 14395-547, Tehran, Iran

2. Université Côte d'Azur, NICE Lab, Parc Valrose 06100 Nice, France

Abstract

By developing the water purification technologies, the usage of superhydrophobic meshes are increased but the fabrication of durable and cost effective superhydrophobic meshes is still challenging. Here, the formation of hierarchical copper fractals on stainless steel meshes and their superhydrophobicity without any physical or chemical modification were studied. In addition, the improvement of superhydrophobicity of surfaces during storing in a glass bottle for a long time (> one year) is reported. The structures were prepared using electrodeposition method applying cyclic voltammetry and square pulse deposition approaches on stainless steel meshes with 50, 100 and 200 microns pore sizes. The prepared layers are a composition of copper with varying amounts of cuprite (Cu_2O) depending on deposition method and mesh pore size. As-prepared cyclic voltammetry layer on 100 microns mesh showed the parahydrophobicity with the contact angle of 154º but a large sliding angle. The one-year stored samples in the glass bottle showed superhydrophobicity with the contact angles larger than 150º and sliding angles in the range of 4º-20º. The observed improvement of superhydrophobicity is a great success in the realm of industrial water purification, while the most other proposed samples by the others have problems related to the durability of superhydrophobicity.

Keywords: Superhydrophobic, Mesh, Dendrite nanostructure, Copper, Electrodeposition

1 Introduction

The water pollution, especially the pollution of seawater caused by huge oil spills, is a great threat for the seas ecosystems and human health. The latest related incident was the Sanchi oil tanker collision and the creation of oil spill as much as Paris area, in the East China Sea. To tackle the issue, various methods have been proposed and used for collecting oil spills including the use of oil- water separation meshes [1-7]. Indeed, a superhydrophobic mesh, which has a porous surface with water repellent

***Corresponding author:**

Thierry Darmanin
E-mail: thierry.darmanin@unice.fr

 property, has special applications in the separation of contamination and oil from water technology. There are many reports which have shown the performance of these meshes in controlled water passing and the separation of organic and petroleum contaminants from water [8-14].

In fact, the wettability of surfaces by liquids has been interested by researchers due to their impact on environmental contamination, durability and the quality of industrial surfaces [15-18]. In the terms of wettability, surfaces are divided into hydrophilic and hydrophobic (similarly, oleophilic and oleophobic) [15]. Superhydrophobic surfaces which minimize the contact angle of liquids can reduce contamination, corrosion and friction due to their ability in repelling water [15-17]. To produce them, the surface energy should be reduced as well as a complicated surface structure with an optimized roughness is needed [15]. Regarding their vast industrial, environmental, and scientific usages such as drag force reduction, anti- icing, anti- bacteria, anti- corrosion, self- cleaning and marine applications, researchers are trying to solve environmental problems by developing this technology [15,16 and18].

Initially, polymers, fatty acids and fluorosiloxan groups were used to reduce the surface energy and to fabricate superhydrophobic meshes for oil-water separation [19-25]. Recently, coating metals on a metal mesh has also been considered as one of the candidates which provide superhydrophobicity [26-35]. This property is mostly obtained by preparing complicated surface structures, including fractals on them, to optimize the water contact angle without any secondary chemical modifications. Nonetheless, the wettability of the as-prepared meshes depends on the pore size, thickness of wires, as well as the surface structure, roughness and chemical composition of the layer. In addition, in practical applications, the stability and durability of the layer is also important especially one uses metals [1-6].

In order to prepare superhydrophobic surface on the stainless steel mesh, we used copper based coatings according to our previous findings [36]. Copper and its oxide family (Cu_xO) have been long used for their optical, electrical, thermal and magnetic properties [37-39]. In addition, the nanometer structure of these materials improves their properties and exhibits unique characteristics of their bulk [40 and 41]. Copper and its oxides can be coated by various chemical or physical processes such as electrodeposition

[26-30,36,39 and 42], radio frequency (RF) sputtering [43], thermal oxidation [44], chemical vapor deposition [45], and sol-gel methods [46]. Among various methods, the electrodeposition of copper can create complicated and different crystalline structures in the sizes of nanometers to micrometers due to its good conductivity [36,39 and 42].

It is shown that the amount of oxygen as well as the growth crystal facet on the surface of copper based layers affects both the surface energy and structure and consequently its hydrophobicity [47]. In fact, decreasing the amount of oxygen in copper oxide samples may increase the surface energy. The order of the surface energy for various facets in the cubic Cu_2O structure varies as: {111} < {110} < {100}[40]. Furthermore, the increase in the contact angle of copper based surfaces with the rest time, probably due to the change in oxygen amount and contamination of the surface or drying time needed for the samples, was observed before [36 and 48-54].

Cu based samples can be grown at large crystallite structures such as cubic, octahedral and their truncated structures [38,40 and 55-57], which can provide well-defined surface structure to make a predictable roughness and wettability of the surface. Fractals are inherently optimal structures in designing complicated structures with good features, which made them desirable in surface science. Due to multiple-dimensional scale, a fractal structure is hierarchical and identifiable. Many experimental works have been done on the preparation of these surfaces to be applied in heat transfer systems, microfluidics and biotechnology [58]. The ordered structures in microfluidics are able to reduce friction, organize the form of droplets on the surface, and control the absorption of biological molecules and cell adhesion [59]. In these structures, the fractal dimension represents the level of self-similarity [60].

In this study, copper based structures were fabricated using electrodeposition method to study the possibility of fabrication of superhydrophobic meshes. The samples with different morphologies including dendrite leaf- like fractals were prepared on stainless steel meshes using cyclic voltammetry and square pulse approaches. The effect of the deposition method on the chemical components, the surface struc-

 tures, and the hydrophobicity of prepared samples were studied by X-ray diffraction, scanning electron microscopy (SEM), and goniometry. The samples were also analyzed after one year storing in order to practice the effect of rest time on the contact angle of samples. In the following, the experimental methods are described. The results and discussion are given in part 3, and finally the conclusion is drawn in the last part.

2 Materials and methods

2.1 Electrodeposition conditions

In this work, stainless steel meshes with 50, 100 and 200 micron pore sizes were coated using cyclic voltammetry and square pulse approaches (SM50, SM100, SM200 CV and Pulse samples). Before coating, substrates were washed with a constant process. At first, they were subjected to ultrasound for 40 minutes in ethanol and then dried in a furnace at 100 ° C for 1 hour. The contact angle of clean meshes was 0, 123 and 110 degrees, for meshes with 50, 100 and 200 µm apparatus, respectively. An Autolab potentiostat of Metrohm was used for the electrochemical experiments in two different methods, cyclic voltammetry, and square pulse deposition, as reported before [36]. A three-electrode system was connected to the potentiostat: stainless steel meshes (50, 100 and 200 micron apertures) as working electrode, a carbon rod as a counter-electrode and a saturated calomel electrode (SCE) as reference electrode. A 0.1 M aqueous $CuSO_4.5H_2O$ (Sigma Aldrich) solution in ultra-pure water was used as electrolyte. 10 mL of this solution was added to the electrochemical glass cell and let degassing during 5 min under argon. After the electrodeposition, the samples were washed in distilled water and dried for one week at ambient conditions before the characterization (Table 1).

2.2 Surface characterization

The water contact angle (θ_w) and sliding angle (θ_{SA}) were measured three times using a DSA30 goniometer (Krüss) with a 2 and 5 μL water droplet (γ_{LV} = 72.8 mN/m) at five different positions on each sample: 2 times after the preparation with one-week-long, and once after a year of preparation. X-ray diffraction (XRD) patterns of the samples were studied by Philips XRD X'pert MPD diffractometer (Cu Kα radiation, 1.54 Å) with step size of 0.02˚ and count time of 1 s per step in 2θ range from 10° to 80° at grazing incidence mode. A 6700F microscope (JEOL) was used to obtain the SEM images.

3 Results

3.1 Cyclic voltammetry

Measured oxidation voltages of prepared samples as the working electrode with different pore size meshes are equal to -0.65, -0.75 and -0.70 for SM50, SM100 and SM200 meshes, respectively. The cyclic voltammetry electrodeposition was done using a fixed negative potential equal to -0.5 V as working potential with a fixed 0 V as positive potential at a scan rate of 20 mV s^{-1} for 1 to 7 cycles of deposition for all three mesh sizes (SM50-CV-1 , 3, 7 , SM100-CV-1,3,7 , and SM200-CV-1,3,7 samples, respectively).

It is extremely important to well characterize the surface chemistry. The presence of copper and cuprite in all samples were observed through the X-ray diffraction pattern of deposited meshes with three numbers of deposition cycles (Fig. 1). The highest peak in all of them belongs to the Cu (111) facets. The second highest peak in SM100-CV-3 and SM200-CV-3 is related to Cu (002). However, the second peak in SM50-CV-3 is Cu_2O (111) with the half height of the main peak, indicating the formation of oxide layer during the deposition. This effect can be the result of a few differences between the oxidation and working voltages of the sample. The height of the same peak in the SM200-CV-3 sample is one quarter of the main peak while this peak is extremely weak in the SM100-CV-3. Additionally, a strong Cu (002) peak is in SM50-CV-3 sample. To summarize, sorting the different samples in accordance with the amount of presented copper and copper oxide phases in the layer, we have: SM100-CV>

[6] SM200-CV> SM50-CV and, SM50-CV> SM200-CV>> SM100-CV, respectively. As it was mentioned in the introduction, the existence of a few amount of oxygen in the SM100-CV layer has more positive effect on the hydrophobicity of the sample than the rest.

The observed fractal structures in the SM200-CV mesh are less similar to the leaves. In these structures big semi- cubic structures with the composition of the 100 to 500 nm crossover cubes were made instead of needle-shaped (long and small diameter) units. The formed structures are clamped to each other irregularly. Of course, in most of the structures, the 5 numbers of branches are still observed. A summary of the prepared structure features is listed in the Table 2.

According to the large scale images in the Fig. 2 (left side), all three samples have been well covered with copper dendrite structures. However, the homogeneity of layer in the SM100-CV sample is more than the rest.

The average contact angle of the water droplet on the surfaces versus the numbers of deposition cycles are shown in Fig. 3a for different pore size meshes. In addition, photographs of the water and sunflower oil droplets on the samples are shown in Fig. 3 b and c. In every curve of Fig. 3a, the contact angle at zero numbers of deposition cycles relates to a clean and uncoated stainless steel mesh. The contact angle of SM50-CV-1, SM50-CV-3 and SM50-CV-7 samples, despite the presence of fractal structures on them, is equal to 0º, the same as the uncoated one. So, it can be concluded that the use of SM50-CV meshes maybe is not suitable for the production of superhydrophobic meshes (this idea will be altered at the end of the results part of this manuscript).

The contact angle of SM100-CV and SM200-CV samples is increased by applying the fractal copper coating. It should be noted that these samples were hydrophobic in their uncoated state (with contact angles of 123º and 110º, respectively). The increase of contact angle compared to uncoated samples in SM100 is higher than the two other mesh sizes. In addition, the contact angle remains approximately constant by increasing the deposition cycles. Two factors can be attributed to this behavior: the uniformity of homogeneous fractal coverage of the SM100-CV sample versus the non-uniformity of in-

homogeneous fractal coverage of the others and the needle- like structure of the sample compared to the cube-tips of other samples. SM100-CV samples are not superhydrophobic (θ_W> 150º and θ_{SA}<72º in as-prepared sample) but parahydrophobic due to large hysteresis, as reported by Marmur [61] and observed on rose petals [62]. That indicates the creation of an intermediate state [63 and 64] between the Wenzel [65] and the Cassie- Baxter [66] states.

However, increasing the numbers of deposition cycles leads to slight reduction of the contact angle of SM200-CV samples. The reduction can be due to the heterogeneity in surface structures of these samples, which is obvious from the SEM images (Fig. 2). Furthermore, at all three sizes of meshes, samples with 5 numbers of deposition cycles are powdery; so, the water droplet contact angle on them is zero due to the absorption and distribution of water in the powdery layer. The repeatability of the obtained results of contact angle was confirmed by re-preparing the samples.

3.2 Square pulse method

Similar to the cyclic voltammetry method presented in the previous part, the square pulse electrodeposition method [36,67 and 68] was used at working potential -0.5 V for 10 s and relaxing for 2 s at 0 V for all three pore size meshes. The numbers of 8, 12, 16 and 20 pulses were used to prepare each set of the samples. The prepared samples have given the name as SM50-Pulse-8, 12, 16, 20, SM100- Pulse-8, 12, 16, 20, and SM200- Pulse-8, 12, 16, 20, respectively. For example, the SM50- Pulse-8 is representative of the samples with 50 micron apertures and 8 pulses.

The X-ray patterns of SM50, 100, and 200 Pulse samples made during 8 square pulses of deposition were shown in the Fig. 4. In all three samples, the highest peak is Cu (111). Moreover, in the SM50-Pulse, there is a large peak at Cu_2O (111) with 80% height against the main peak. It should be noted that these samples, found a slightly powdery state, which is lower in the 8 pulse sample (SM50-Pulse -8). The second highest peak In SM100-Pulse and SM200-Pulse meshes is Cu (002), which indicates the low amount adsorption of oxygen in the layer. As it was shown before by re-

 searchers, the surface energy is reduced when the amount of oxygen is reduced in Cu_xO [47]. Hence, the water repellency of the layer is improved.

It is expected that the hydrophobicity of coated stainless steel meshes improves by increasing the copper compounds thickness of the composition on SM100-Pulse and SM200-Pulse meshes. However, the amount of cuprite in the layer is significant in SM50-Pulse sample. In fact, during the deposition of copper layer on the samples with different parameters and the same voltage, the voltage is closer to the oxidation voltage of the SM50-Pulse than two others. Consequently, the possibility of the formation of oxide layers on this mesh is higher than that of the others. Based on the Fig. 4, the intensity of copper and cuprite peaks is according to I(111)> I(002)> I(022) in different orientations. This behavior indicates that the preferred growth is in the direction of the diameter of the crystalline structures of these two materials [40].

As shown in Fig. 5, there are hierarchical structures on SM50-Pulse that indicate fractal growth of the surface. The length of the branches is also 2-3 μm and the base diameter is less than two microns. However, formed structures on the SM100 and 200 -Pulse surfaces are similar.

Based on the right sided images in the Fig. 5, the formed structure on the SM100-Pulse is larger and more distinctive, having micrometric valleys between the structures. Consequently, because of larger contact angle in clean state of SM100-Pulse mesh, the larger contact angle is expected compared to that of the others after the deposition of copper layer on it. Still, the less complexity on the surface compared to the cyclic voltammetry sample may cause the droplet to stick on the surface structure and not to detach.

Fig. 6 depicts the contact angle data in zero pulse representing the initial contact angle of the meshes without the deposition. The increase in the water contact angle of the surface of SM50- Pulse-8 is observed. The mentioned sample (SM50 mesh) is superhydrophilic without the deposition.

The observed contact angle is approximately equal to the contact angle of a smooth layer of copper, has been observed previously [36]. Therefore, it is expected that a mesh with small pore size acts as a flat surface in this case.

By increasing the deposition, the layer converted into the powdery state. The contact angles of these samples are zero because of the spreading of the droplet in the powder. The 17 degrees increase of contact angle was obtained after the deposition of copper on the surface for the SM200-Pulse mesh. In the SM200-Pulse, an approximately unchanged contact angle (around 125º) was observed by increasing the deposition. It means that maybe no significant change was happened in the surface structure with the increase of the thickness. In the as-prepared SM100-Pulse samples, the contact angle of 8 pulse sample reached to 150º. However, regardless of the large contact angle, it is not a superhydrophobic layer as a result of the adhesion of the droplet to the surface but is parahydrophobic [61] as observed by cyclic voltammetry. In addition, increasing the deposition will lead to the decrease of contact angle to zero. It may be due to the powdering of 16 and 20 pulse samples.

3.3 The improvement of samples wetting by the rest time

As we did not modify our surfaces with a hydrophobic monolayer such as a hydrophobic thiol or silane, it could be expected that the contact angle changes over the time because the surface chemistry of copper and copper oxides is sensitive to different stimuli [51-54 and 69-71]. Regarding our recent observation, the hydrophobicity of prepared copper layers are improved by storing for a long time in a closed glass bottle [36, 51 and 52]. We had previously checked this phenomenon systematically in our works [36 and 52] for some weeks after the sample preparation. It is observed that the increase in the water droplet contact angle on the surface will be saturated after a time, depending on its available surface under the air exposure. Hence, contact angle of selected samples was measured after one year. The results were exciting. All the samples showed the superhydrophobicity with the contact angle higher than 150º and sliding angles less than 20º (Table 3). As it was mentioned in the literature [48-50,

[10] 52 and 54] it can be due to desorption of oxygen from the layer, and therefore decreasing the surface energy of the surface. Moreover, the reduction of the layer surface energy will increase the hydrophobicity. The ex- superhydrophilic was observed for SM50 samples coated by cyclic voltammetry method. Actually the surface did not show the powdery state again after one year storing, which is obvious from the sample. Still, the factors affecting the increase of superhydrophobicity of the samples need more studies. Some literatures [51, 53, 54 and 71] proposed that the detection of the change of adsorbed oxygen in the layer is difficult regarding to the penetration depth of the ordinary chemical composition characterization methods (XPS, FTIR, EDAX, PL and etc.). Moreover, the corresponding peaks of copper and Cu_xO in these methods are overlapped.

It has been reported so far that the hydrophobicity of most of prepared samples, especially meshes used for oil- water separation are challenging by the rest time [1-5]. Therefore, the increase in the hydrophobicity of our prepared meshes can be very useful in fabrication of superhydrophobic metal based meshes to be used in water purification industries.

4 Discussions

According to the aforementioned results, different microstructures including dendrite leaves were formed on the steel meshes during the electrodeposition of copper. In this work, the cyclic voltammetry and square pulse approaches were used. In SM50 and SM100 meshes coated by the cyclic voltammetry method, surface was covered by leaf-like fractal structures. They have micrometric length with 5 to 6 branches around the tip of leafs. In addition, SM100-CV samples were more needle like than SM50-CV samples and had more homogenous coverage on the mesh surfaces. In SM200-CV samples fractals were made by an aggregation of semi-cubic structures in different sizes from 500 nm to 3 μm, which had less repeatability of structures than the two last samples (SM50-CV and SM100-CV). The XRD patterns of CV samples surfaces showed a composition of copper facets and a few amount of Cu_2O, which is negligible in SM100- CV sample. So, in CV samples the as- prepared SM100-CV-3 mesh shows the

parahydrophobicity that means high contact angle but also high hysteresis and sliding angles. In the pulse deposited samples, the fractal structures are formed only in SM50-Pulse surfaces with less repetition than CV samples. Whereas, in SM100-Pulse and SM200-Pulse samples, similar structures are formed due to the aggregation of cubes in different sizes, with deep valleys between structures. Less complicated structures in SM100-Pulse than SM100-CV samples cause the adhesion of water droplet on the surface, despite a large contact angle. In addition, according to the XRD analysis results, pulse samples have more cuprite in the structure than the CV samples. An interesting effect that has been observed is to reach superhydrophobicity with low hysteresis and sliding angle with a rest in a sealed glass box. In addition, although as- prepared structures on SM50 meshes were powdery and the water droplet spread on it, the situation was changed after a long time resting in a sealed box; the samples were no longer powder and they became superhydrophobic. This phenomenon can be due to desorption of oxygen in the layers by the rest time in a sealed box. Therefore, it seems that the superhydrophobicity in meshes coated by complicated dendrite copper based structures occur in two different conditions: 1- First with the formation of dendrite hierarchical structures, the hydrophobicity of surface is increased (structural dependence), and 2. Superhydrophobicity will be improved by resting and structural strength of the samples which may be due to the decrease of adsorbed oxygen amount in the surface. So, in the second condition, the type of the surface complexity is not the main factor in superhydrophobicity and the complexity of the surface is just sufficient.

5 Conclusions

In summary, the superhydrophobic stainless steel meshes with different pore sizes have been prepared. The samples were coated by copper based hierarchical structures including dendrite leaves on them using the cyclic voltammetry and square pulse approaches of the electrodeposition method. It was observed that the morphology and chemical composition of the prepared samples changes by varying the applied deposition method. In addition, a sharp increase in superhydrophobicity of the surfaces by

 the rest time without any physical or chemical modification were observed which has a huge advantage in the application of these samples in the industry. It is well known that the major concerns about the use of superhydrophobic meshes in the industry are the reduction of their superhydrophobicity over the time. So, it is expected that preparation of these meshes in larger sizes can be a promise in the industrial field, in the contamination separation from water in the industries.

Acknowledgments

Partial financial support by the Research Council of the University of Tehran and Iranian National Science Foundation under grant # 95849613 is acknowledged. The authors also thank the Iran nano-technology initiative council and the Centre Commun de Microscopie Appliquée (CCMA), Nice, France, for the SEM images.

References

[1] Wang L K, Hung Y T, Shammas N K. *Advanced Physicochemical Treatment Processes, Chapter 16: Oil Water Separation*. Humana Press, New Jersey, USA, 2006.

[2] Xue Z. , Cao Y, Liu N, Feng L, Jiang L. Special wettable materials for oil/water separation. *Journal of Materials Chemistry,* 2014, **2**, 2445–2460.

[3] Padaki M, Surya Murali R, Abdullah M S, Misdan N, Moslehyani A, Kassim M A, Hilal N, Ismail A F. Membrane technology enhancement in oil–water separation. A review. *Desalination,* 2015, **357**, 197–207.

[4] Zhu Y, Wang D, Jiang L, Jin J. Recent progress in developing advanced membranes for emulsified oil/water separation. *NPG Asia Materials,* 2014, **6**, e101.

[5] Gupta R K, Dunderdale G J, England M W, Hozumi A. Oil/water separation techniques: a review of recent progresses and future directions. *Journal of Materials Chemistry A,* 2017, **5**, 16025– 16058.

[6] Chu Z, Feng Y, Seeger S. Oil/water separation with selective superantiwetting/superwetting surface materials. *Angewandte Chemie International Edition,* 2015, **54**, 2328-2338.

[7] Wang S, Song Y, Jiang L. Microscale and nanoscale hierarchical structured mesh films with superhydrophobic and superoleophilic properties induced by long-chain fatty acids. *Nanotechnology,* 2007, **18**, 015103- 015107.

[8] La D D, Nguyen T A, Lee S, Kim J W, Kim Y S. A stable superhydrophobic and superoleophilic Cu mesh based on copper hydroxide nanoneedle arrays. *Applied Surface Science,* 2011, **257**, 5705–5710.

[9] Wang C, Yao T, Wu J, Ma C, Fan Z, Wang Z, Cheng Y, Lin Q, Yang B. Facile Approach in Fabricating Superhydrophobic and Superoleophilic Surface for Water and Oil Mixture Separation. *ACS Applied Materials & Interfaces,* 2009, **1**, 2613–2617.

[10] Pan Q, Wang M, Wang H. Separating small amount of water and hydrophobic solvents by novel

superhydrophobic copper meshes. *Applied Surface Science,* 2008, **254**, 6002–6006.
[11] Tian D, Zhang X, Wang X, Zhai J, Jiang L. Micro/nanoscale hierarchical structured ZnO mesh film for separation of water and oil. *Physical Chemistry Chemical Physics,* 2011, **13**, 14606–14610.
[12] Wang C F, Tzeng F S, Chen H G, Chang C J. Ultraviolet-Durable Superhydrophobic Zinc Oxide-Coated Mesh Films for Surface and Underwater−Oil Capture and Transportation. *Langmuir,* 2012, **28**, 10015–10019.
[13] Moura F C C, Lago R M. Catalytic growth of carbon nanotubes and nanofibers on vermiculite to produce floatable hydrophobic ‘‘nanosponges’’ for oil spill remediation. *Applied Catalysis B: Environmental,* 2009, **90**, 436- 440.
[14] Sun Z, Liao T, Li W, Dou Y, Liu K, Jiang L, Kim S W, Kim J H, Dou S X. Fish-scale bio-inspired multifunctional ZnO nanostructures. *NPG Asia Materials*, 2015, **7**, e232, 1-9.
[15] Darmanin T., Guittard F. *Bioinspired Superhydrophobic Surfaces: Advances and Applications with Metallic and Inorganic Materials.* Pan, Stanford, USA, 2017.
[16] Zhang P, Lv FY. A review of the recent advances in superhydrophobic surfaces and the emerging energy-related applications. *Energy,* 2015, **82**, 1068–1087.
[17] Liu J, Huang X, Li Y, Li Z, Chi Q, Li G. Formation of hierarchical CuO microcabbages as stable bionic superhydrophobic materials via a room-temperature solution-immersion process. *Solid State Sci*ence, 2008, **10**, 1568–1576.
[18] Si Y, Guo Z. Superhydrophobic Nanocoatings: From Materials to Fabrications and to Applications. *Nanoscale,* 2015, **7**, 5922–5946.
[19] Darmanin T, Guittard F. Homogeneous growth of conducting polymer nanofibers by electrodeposition for superhydrophobic and superoleophilic stainless steel meshes. *RSC Advances,* 2014, **4**, 50401–50405.
[20] Saltuganov P N, Ionin A A, Kudryashov I, Rukhadze A A, Gavrilov A I, Makarov S V, Rudenko A A, Zayarny D A. Fabrication of superhydrophobic coating on stainless steel surface by femtosecond laser texturing and chemisorption of an hydrophobic agent. *Journal of Russian Laser Research,* 2015, **36**, 81–85.
[21] Wang S, Song Y, Jiang L. Microscale and nanoscale hierarchical structured mesh films with superhydrophobic and superoleophilic properties induced by long-chain fatty acids. *Nanotechnology,* 2007, **18**, 015103- 015107.
[22] Crick C R, Gibbins J A, Parkin I P. Superhydrophobic polymer-coated copper-mesh; membranes for highly efficient oil–water separation. *Journal of Materials Chemistry A,* 2013, **1**, 5943–5948.
[23] Yu S, Guo Z. Superhydrophobic surfaces based on polypyrrole with corrosion resistance and the separation of Oil/Water mixtures properties. *RSC Advances,* 2015, **5**, 107880–107888.
[24] Dou Y, Tian D, Sun Z, Liu Q, Zhang N, Kim J H, Jiang L, Dou S X. Fish gill inspired cross flow for efficient and continuous collection of spilled oil, *ACS Nano*, 2017, **11**, 2477-2485.
[25] Sun Z, Liao T, Liu K, Jiang L, Kim J H, Dou S X. Robust superhydrophobicity of hierarchical ZnO hollow microspheres fabricated by two-step self-assembly. *Nano Research,* 2013, **6**, 726-735.
[26] Zhao Y, Xiao X, Ye Z, Ji Q, Xie W. Fabrication of durable copper plating superhydrophobic surface with improved corrosion resistance and oil–water separation properties. *Applied Physics A,* 2018, **124**, 193- 202.
[27] Li J, Long Y, Xu C, Tian H, Wu Y, Zha F. Continuous, high-flux and efficient oil/water separation

assisted by an integrated system with opposite wettability. *Applied Surface Science,* 2018, **433**, 374–380.

[28] Liu Y, Zhang K, Yao W, Zhang C, Han Z, Ren L. A Facile Electrodeposition Process for the Fabrication of Superhydrophobic and Superoleophilic Copper Mesh for Efficient Oil−Water Separation. *Industrial & Engineering Chemistry Research,* 2016, **55**, 2704–2712.

[29] Jain R, Pitchumani R. Facile Fabrication of Durable Copper Based Superhydrophobic Surfaces via Electrodeposition. *Langmuir,* 2018, **34**, 3159–3169.

[30] Song J, Huang S, Lu Y, Bu X, Mates J E, Ghosh A, Ganguly R, Carmalt C J, Parkin I P, Xu W, Megaridis C M. Self-Driven One-Step Oil Removal from Oil Spill on Water via Selective-Wettability Steel Mesh. *ACS Applied Materials & Interfaces,* 2014, **6**, 19858–19865.

[31] Song Y, Liu Y, Zhan B, Kaya C, Stegmaier T, Han Z, Ren L. Fabrication of Bioinspired Structured Superhydrophobic and Superoleophilic Copper Mesh for Efficient Oil-water Separation. *Journal of Bionic Engineering,* 2017, **14**, 497–505.

[32] Raturi P, Yadav K, Singh J P. ZnO-Nanowires-Coated Smart Surface Mesh with Reversible Wettability for Efficient On-Demand Oil/Water Separation. *ACS Applied Materials & Interfaces,* 2017, **9**, 6007−6013.

[33] Guo J, Yang F, Guo Z. Fabrication of stable and durable superhydrophobic surface on copper substrates for oil–water separation and ice-over delay. *Journal of Colloid and Interface Science,* 2016, **466**, 36–43.

[34] Sang Y C, Albadarin A B, Al-Muhtaseb A H, Mangwandi C, McCracken J N, Bell S E J, Walker G M. Properties of Super-Hydrophobic Copper and Stainless Steel Meshes: Applications in Controllable Water Permeation and Organic Solvents/Water Separation. *Applied Surface Science,* 2015, **335**, 107-114.

[35] Gao X, Guo Z. Biomimetic superhydrophobic surfaces with transitional metals and their oxides: a review. *Journal of Bionic Engineering*, 2017, **14**, 401-439.

[36] Akbari R, Ramos Chagas G, Godeau G, Mohammadizadeh M R, Guittard F, Darmanin T. Intrinsically water-repellent copper oxide surfaces; An electrocrystallization approach. *Applied Surface Science*, 2018, **443**, 191-197.

[37] Lee S, Kim K S, Pippel E, Kim S, Kim J H, Lee H J. Facile route toward mechanically stable superhydrophobic copper using oxidation−reduction induced morphology changes. *The Journal of Physical Chemistry C,* 2012, **116**, 2781–2790.

[38] Ding Y, Li Y, Yang L, Li Z, Xin W, Liu X, Pan L, Zhao J. The fabrication of controlled coral-like Cu_2O films and their hydrophobic property. *Applied Surface Science*, 2013, **266**, 395–399.

[39] Dini J W, Snyder D D, *Electrodeposition of Copper, in Modern Electroplating*- 5th Edition, eds M. Schlesinger, M. Paunovic, John Wiley & Sons, Inc., Hoboken, NJ, USA, 2010.

[40] Shirtcliffe N J, McHale G, Newton M I, Perry C C. Wetting and wetting transitions on copper-based super-hydrophobic surfaces. *Langmuir,* 2005, **21**, 937- 943.

[41] Zhao W, Fu W, Yang H, Tian C, Li M, Li Y, Zhang L, Sui Y, Zhou X, Chen H, Zou G. Electrodeposition of Cu_2O films and their photoelectrochemical properties. *CrystEngComm,* 2011, **13**, 2871–2877.

[42] Casella I G, Gatta M. Anodic electrodeposition of copper oxide:hydroxide films by alkaline solutions containing cuprous cyanide ions. *Journal of Electroanalytical Chemistry,* 2000, **494**, 12–20.

[43] Aytug T, Bogorin D F, Paranthaman P M, Mathis J E, Simpson J T, Christen D K. Superhydrophobic ceramic coatings enabled by phase-separated nanostructured composite TiO_2–Cu_2O thin films. *Nanotechnology*, 2014, **25**, 245601- 245607.

[44] kong L, Chen X H, Yu L G, Wu Z S, Zhang P Y. Superhydrophobic cuprous oxide nanostructures on phosphor- copper meshes and their oil−water separation and oil spill cleanup. *ACS Applied Materials & Interfaces*, 2015, **7**, 2616–2625.

[45] Hassan I A, Parkin I P, Nair S P, Carmalt C J. Antimicrobial activity of copper and copper(I) oxide thin films deposited via aerosol-assisted CVD. *Journal of Materials Chemistry B*, 2014, **2**, 2855–2860.

[46] Eskandari A, Sangpour P, Vaezi M R. Hydrophilic Cu_2O nanostructured thin films prepared by facile spin coating method: Investigation of surface energy and roughness. *Materials Chemistry and Physics*, 2014, **147**, 1204–1209.

[47] Maimaiti Y, Nolan M, Elliott S D. Reduction mechanisms of the CuO(111) surface through surface oxygen vacancy formation and hydrogen adsorption. *Physical Chemistry Chemical Physics*, 2014, **16**, 3036–3046.

[48] Chang F M, Cheng S L, Hong S J, Sheng Y J, Tsao H K. Superhydrophilicity to superhydrophobicity transition of CuO nanowire films. *Applied Physics Letters*, 2010, **96**, 114101–114103.

[49] Preston D J, Miljkovic N, Sack J, Enright R, Queeney J, Wang E N. Effect of hydrocarbon adsorption on the wettability of rare earth oxide ceramics. *Applied Physics Letters*, 2014, **105**, 1601–1605.

[50] Zhou C, Li H, Lin J, Hou K, Yang Z, Pi P, Xu S, Wen X, Cheng J. Matchstick-like Cu_2S@Cu_xO nanowiref: transition of superhydrophilicity to superhydrophobicity. *The Journal of Physical Chemistry C*, 2017, **121**, 19716–19726.

[51] Akbari R, Mohammadizadeh M R, Khajeh Aminian M, Abbasnejad M. Hydrophobic Cu_2O surfaces prepared by chemical bath deposition method. *Applied Physics A*, 2019, **125**, 190- 196.

[52] Akbari R, Godeau G, Mohammadizadeh M R, Guittard F, Darmanin T. Fabrication of superhydrophobic hierarchical surfaces by square pulse electrodeposition. *ChemPlusChem*, 2019, **84**, 368-373.

[53] Tam J, Feng B, Ikuhara Y, Ohta H, Erb U. Robust hydrophobic rare earth oxide composite electrodeposits. *Advanced Materials Interfaces*, 2017, **1700850**, 1-11.

[54] Azimi G, Dhiman R, Kwon H, Paxson A T, Varanasi K K. Hydrophobicity of rare-earth oxide ceramics, *Nature Materials*, 2013, **12**, 315-320.

[55] Siegfried M J, Choi K S. Directing the architecture of cuprous oxide crystals during electrochemical growth. *Angewandte Chemie*, 2005, **117**, 3282–3287.

[56] Siegfried M J, Choi K S. Elucidation of an overpotential-limited branching phenomenon observed during the electrocrystallization of cuprous oxide. *Angewandte Chemie International Edition*, 2008, **47**, 368–372.

[57] Hua Q, Shang D, Zhang W, Chen K, Chang S, Ma Y, Jiang Z, Yang J, Huang W. Morphological evolution of Cu_2O nanocrystals in an acid solution: stability of different crystal planes. *Langmuir*, 2011, **27**, 665–671.

[58] Sadana A, *Biosensors: Kinetics of Binding and Dissociation Using Fractals*, Elsevier, Amsterdam, Netherlands, 2003.

[59] Chen X, Li T, Shen J, Hu Z. Fractal design of microfluidics and nanofluidics—a review. *Chemometrics and Intelligent Laboratory Systems*, 2016, **155**, 19–25.
[60] Peitgen H and Saupe D : Editors, *The Science of Fractal Images*, Springer, New york, USA, 1988.
[61] Marmur A. Hydro- hygro- oleo- omni-phobic? Terminology of wettability classification. *Soft Matter,* 2012, **8**, 6867–6870.
[62] Feng L, Zhang Y, Xi J, Zhu Y, Wang N, Xia F, Jiang L. Petal effect: a superhydrophobic state with high adhesive force. *Langmuir,* 2008, **24**, 4114–4119.
[63] Szczepanski C R, Darmanin T, Guittard F. Recent advances in the study and design of parahydrophobic surfaces: from natural examples to synthetic approaches. *Advances in Colloid and Interface Science*, 2017, **241**, 37–61
[64] Bhushan B, Nosonovsky M. The rose petal effect and the modes of superhydrophobicity. *Philosophical Transactions of the Royal Society A*, 2010, **368**, 4713–4728.
[65] Wenzel R N. Resistance of solid surfaces to wetting by water. *Industrial & Engineering Chemistry Research*, 1936, **28**, 988–994.
[66] Cassie A B D, Baxter S. Wettability of porous surfaces. *Transactions of the Faraday Society,* 1944, **40**, 546–551.
[67] Ramos Chagas G, Akbari R, Godeau G, Mohammadizadeh M R, Guittard F, Darmanin T. Electrodeposited poly(thieno[3,2-b]thiophene) films for the templateless formation of porous structures by galvanostatic and pulse deposition. *ChemPlusChem*, 2017, **82**, 1351–1358.
[68] Karami H, Asadi M G, Mansoori M. Pulse electropolymerization and the characterization of polyaniline nanofibers. *Electrochimica Acta*, 2012, **61**, 154–164.
[69] Wang R, Hashimoto K, Fujishima A, Chikuni M, Kojima E, Kitamura A, Shimohigoshi M, Watanabe T. Light-induced amphiphilic surfaces. *Nature*, 1997, **388**, 431-432.
[70] Wang R, Hashimoto K, Fujishima A, Chikuni M, Kojima E, Kitamura A, Shimohigoshi M, Watanabe T. Photogeneration of highly amphiphilic TiO_2 surfaces. *Advanced Materials*, 1998, **10**, 135-138.
[71] Tu S H, Wu H C, Wu C J, Cheng S L, Sheng Y J, Tsao H K. Growing hydrophobicity on a smooth copper oxide thin film at room temperature and reversible wettability transition. *Applied Surface Science*, 2014, **316**, 88-92.

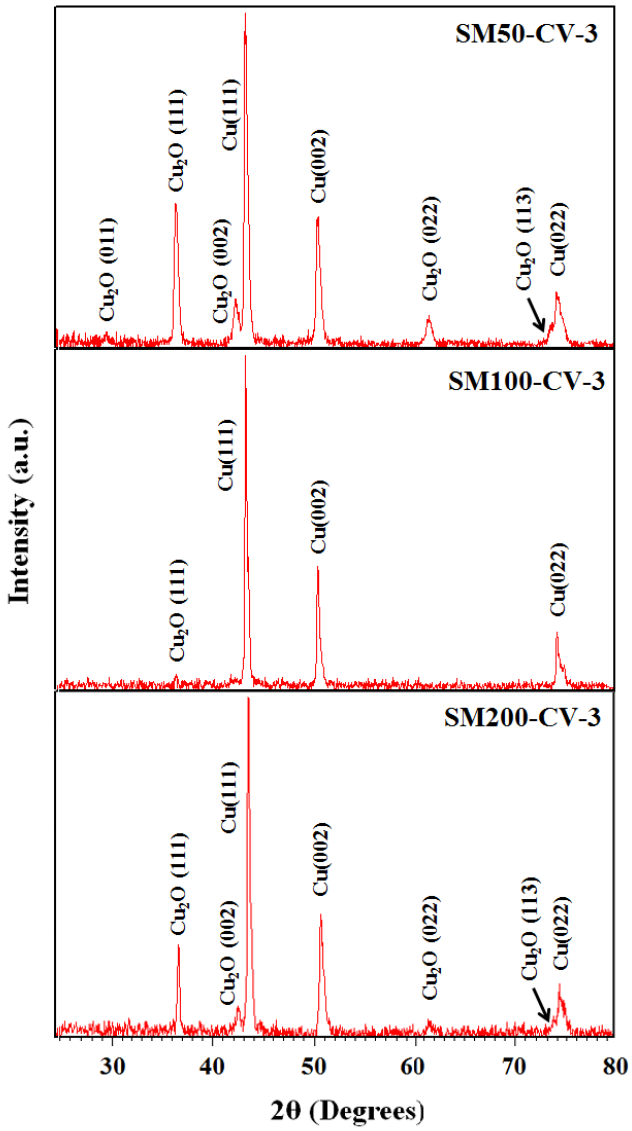

Fig. 1. X-ray diffraction pattern of layers made on stainless steel meshes with various pore sizes.

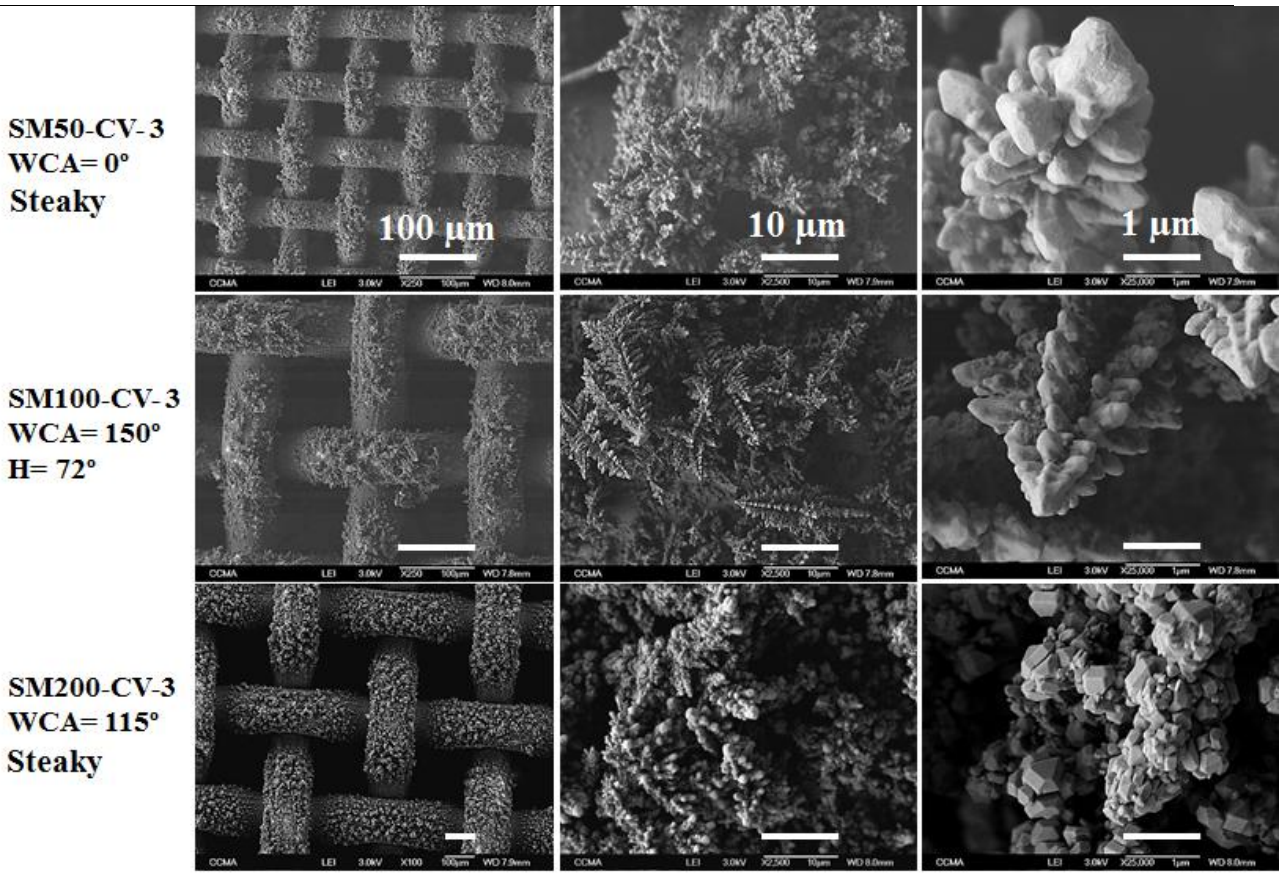

Fig. 2. SEM images from the surface of the mesh samples prepared with three numbers of deposition cycles, in three image magnification windows. At the left of the images, the contact angle data is available for each sample. WCA and H represent the contact and sliding angles of the water droplet on the as-prepared surfaces, respectively.

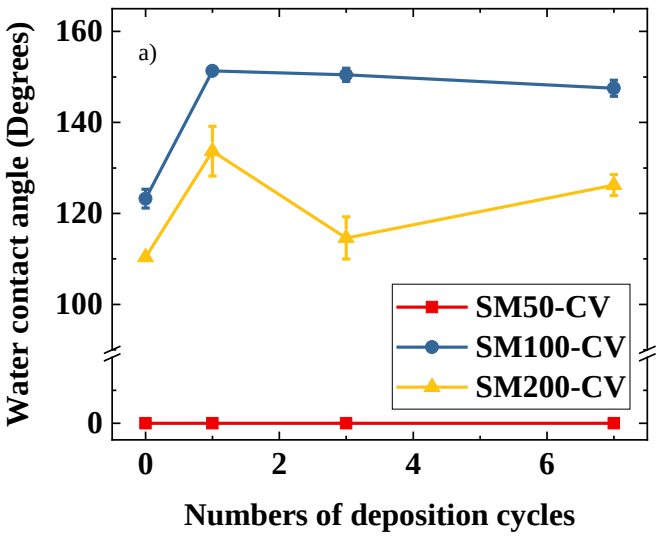

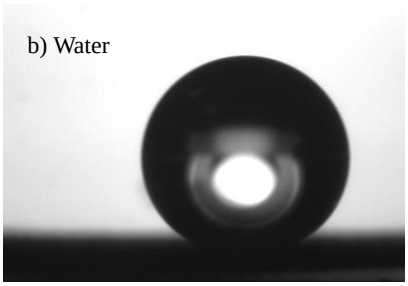

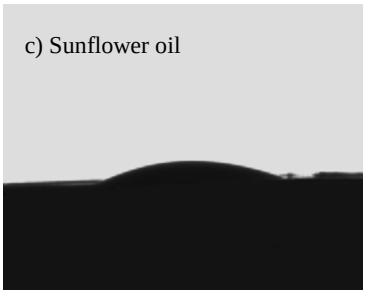

Fig. 3. a) The changes in water contact angle on the meshes with different pore sizes in various numbers of deposition cycles. b and c) The photograph of the water and oil (before penetration through the mesh) droplets on the SM100-CV- 3 surface.

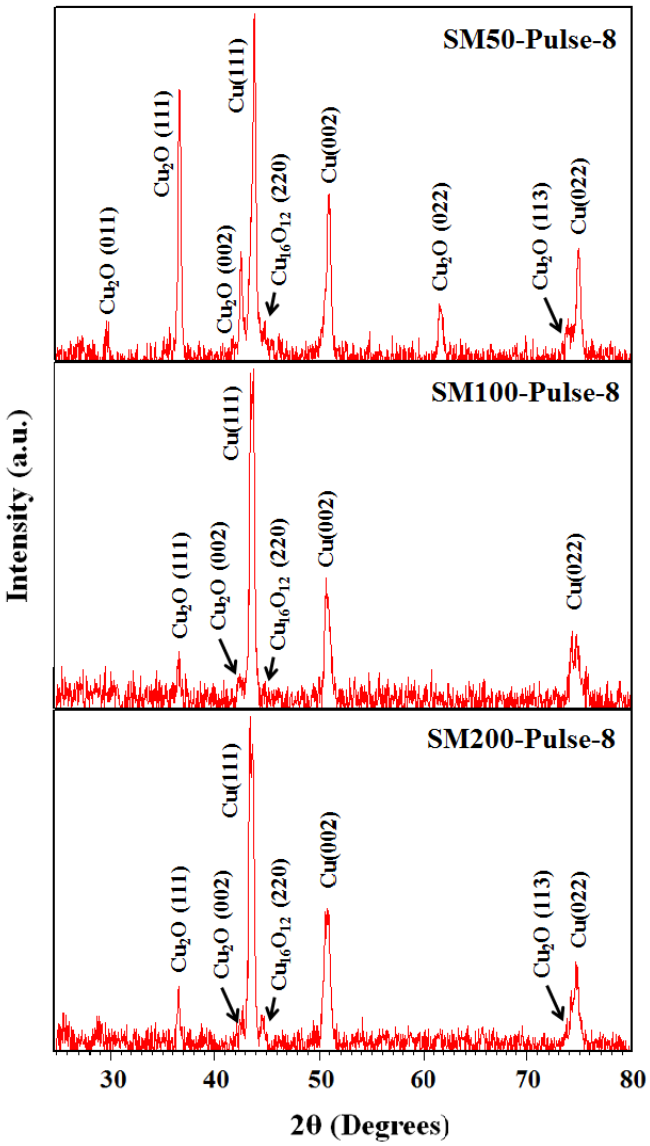

Fig. 4. X-ray diffraction patterns of prepared samples by square pulse deposition method on stainless steel meshes with different pore sizes.

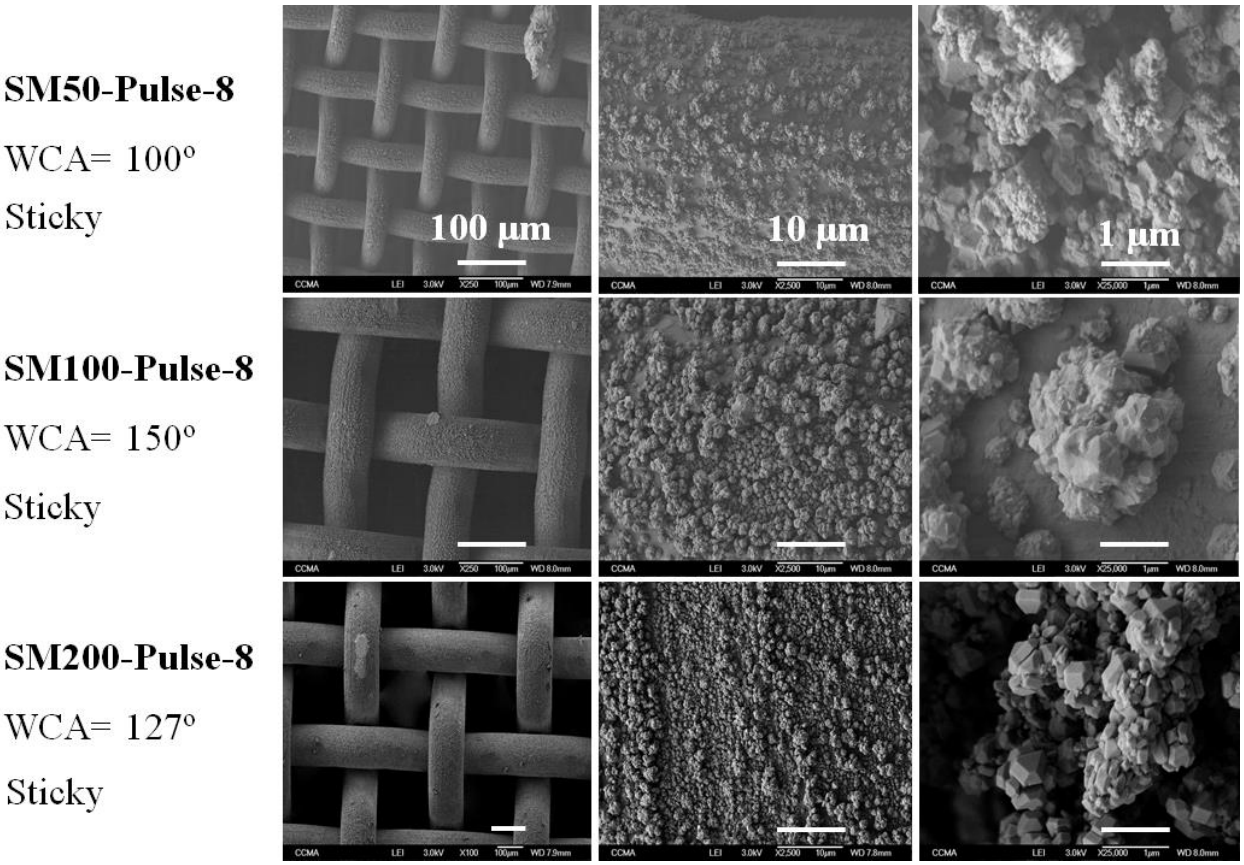

Fig. 5. Scanning electron microscopy images of prepared samples by square pulse method on meshes with different pore sizes.

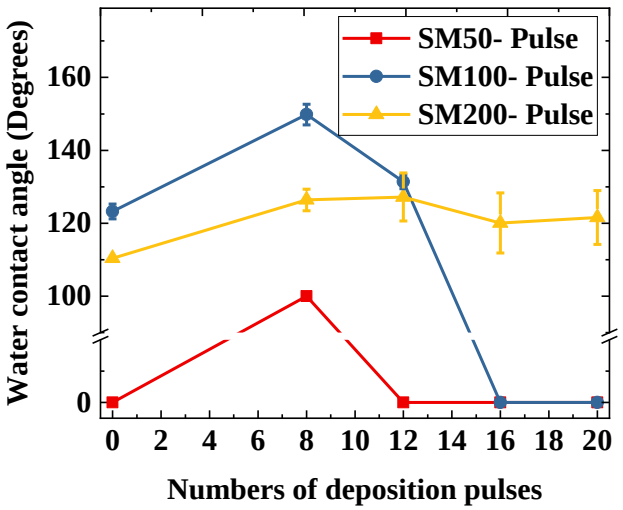

Fig. 6. The water contact angle on the as- prepared samples with square pulse method on meshes with different pore sizes.

Table 1. Sizes of stainless steel meshes with less than ±5 μm error in pore sizes and wire diameters.

Meshes	Average pore size (μm)	Average wire diameter (μm)	Open area (%)	Lines per inch (#)	Average θ_w on uncoated mesh (º)
SM50	48	35	36%	#280	0
SM100	98	70	35%	#140	123
SM200	200	140	35%	#70	110

Table 2. Change in the dimensions of the structures created on the meshes with different pore sizes.

Pore size (μm)	50	100	200
The range of trunk length (μm)	2-4	6-9	2-3
The length of nanostructured leaf (μm)	0.6	1	0.5
The diameter of nanostructured leaf (μm)	0.6	0.35	0.5
The numbers of fractal branches around the trunk	5	5 & 6	5

Table 3. The change in contact and sliding angles of as-prepared samples and after one year storing in a sealed glass bottle. Each of the measured contact and sliding angles have ±3º and ±1º error bars, respectively.

Sample	As- prepared samples		After one year storing in a glass bottle	
	Contact angle(º)	Sliding angle(º)	Contact angle(º)	Sliding angle(º)
SM50-CV- 3	0	Sticky	149	8
SM50-Pulse - 8	0	Sticky	154	5
SM100-CV - 3	150	72	154	15 to less than 4
SM100-Pulse - 8	150	Sticky	156	20
SM200-CV - 3	115	Sticky	159	4
SM200-Pulse - 8	126	Sticky	150	16